Supporting Information

Immunometabolic reprogramming of macrophages by miR-423-5p-enriched small extracellular vesicles delivered via glucose/ROS-responsive hydrogel for diabetic wound healing

Meihua Chen [1#], Qianru Guo[3#], Ziyang Qin[1], Zihan Tang[1], Junjie He[1], Tao Xiang[3*], Hongjuan Cui[1, 2*]

[1] State Key Laboratory of Silkworm Genome Biology, Medical Research Institute, Southwest University, Chongqing, 400716, China;

[2] Jinfeng Laboratory, Chongqing, China;

[3] Institute of Biomedical Engineering, College of Medicine, Southwest Jiaotong University, Chengdu 610031, China.

[#] These two authors contributed equally in this work.

*Corresponding author: Hongjuan Cui, Ph. D.

China Tel: +86 18523178903; Email: hcui@swu.edu.cn

*Corresponding author: Tao Xiang, Ph. D.

China Tel: +86 13608014195; Email: xita198906@swjtu.edu.cn

Materials

Carboxymethyl chitosan (CMCS, carboxylation degree ≥ 80%, degree of deacetylation ≥ 90%, Mw = 150 - 800 kDa) was obtained from Shanghai Yuanye Bio-Technology Co., Ltd. (China). Hyaluronic acid (HA, Mw =1300~1500 kDa) was purchased from Bloomage Biotechnology Co., Ltd. (China). Dextran (DEX, Mw = 20 kDa), 4-aminophenylboronic acid (APBA), and ethylene glycol were purchased from Shanghai Aladdin Biochemical Technology Co., Ltd. (China). Sodium periodate ($NaIO_4$), N-(3-dimethylaminopropyl)-N′-ethylcarbodiimide hydrochloride (EDC·HCl), and N-hydroxysuccinimide (NHS) were obtained from Adamas (China). Phosphate-buffered saline (PBS) and Dulbecco's modified Eagle medium (DMEM) were obtained from Gibco (USA). Serum-free medium was bought from Umibio, (China). PKH26 was bought from MCE (USA). Macrophage colony-stimulating factor (M-CSF) was bought from ABclonal (China). Fetal bovine serum (FBS) was purchased from Hyclone and Gibco (USA). Glucose was bought from Sigma-Aldrich (USA). MitoSOX™ Green was supplied by Thermo Fisher (USA). BODIPY 493/503 was bought from MCE (USA). 5-ethynyl-2′-deoxyuridine (EdU), FAO assay kit was bought from Pumei Biotechnology (China). JC-1 probe, ROS assay kits and Dihydroethidium (DHE) probe were supplied by Beyotime Biotechnology Co., Ltd. (China).

Cell Culture

ADSCs were isolated from discarded adipose tissue obtained from healthy donors undergoing liposuction. Briefly, adipose tissue was washed extensively with PBS

containing 1% penicillin-streptomycin, minced into small fragments, and enzymatically digested with collagenase type I (2.5 mg mL^{-1}) at 37 °C for 60 min with gentle agitation. The digestion was terminated by adding DMEM supplemented with 10% FBS. The cell suspension was filtered through a 70-μm cell strainer and centrifuged at 300 × g for 10 min to obtain the stromal vascular fraction. Cells were resuspended and cultured in DMEM supplemented with 10% FBS and 1% penicillin-streptomycin at 37 °C in a humidified atmosphere containing 5% CO_2. The medium was changed every 2-3 days.

UCMSCs were derived from Wharton's jelly of full-term umbilical cords obtained from healthy neonates delivered by cesarean section, with maternal informed consent and ethical approval. Umbilical cords were rinsed repeatedly with PBS under sterile conditions, and Wharton's jelly was dissected and minced into 1 mm^3 fragments. Tissue explants were evenly placed in culture flasks and maintained in α-MEM supplemented with 10% FBS. After 5-7 days of static culture, cells migrating from the explant edges were collected and expanded. Cells exhibited a homogeneous fibroblast-like morphology, expressed standard mesenchymal stem cell surface markers, and possessed multi-differentiation potential.

Culture of BMDMs, HUVECs, and HaCaT cells

BMDMs were isolated from femurs and tibiae of 6- to 8-week-old C57BL/6 mice. Bone marrow cells were flushed with PBS, filtered through a 70 μm cell strainer, and cultured in RPMI 1640 medium containing 10% FBS, 1% penicillin-streptomycin, and 50 ng/mL M-CSF for 5 days to induce macrophage differentiation.

HUVECs and HaCaT cells were purchased from the American Type Culture Collection (ATCC) and maintained in RPMI 1640 medium supplemented with 10% FBS and 1% penicillin-streptomycin at 37 °C in 5% CO_2. To establish a hyperglycemic model, cells were treated with 35 mM glucose for 48 h. For EVs treatment, cells at 80% confluence were incubated with 100 μg mL^{-1} EVs derived from ADSCs or UCMSCs.

Cell Proliferation Assay

Cell proliferation was assessed using the EdU assay. Cells seeded in 24-well plates were treated with 100 μg mL^{-1} EVs for 24 h at 60-80% confluence, then incubated with 10 μM EdU for 2 h. Cells were fixed with 4% paraformaldehyde, permeabilized with 0.3% Triton X-100, and stained using a Click-iT EdU detection kit according to the manufacturer's instructions. Nuclei were counterstained with Hoechst. EdU-positive cells were visualized under a fluorescence microscope and quantified by mean fluorescence intensity using ImageJ.

Scratch Wound Assay

HUVECs or HaCaT cells were seeded at high density (1×10^6 cells $well^{-1}$) in 12-well plates and grown to confluence. A straight scratch was created using a sterile 200 μL pipette tip. After washing with PBS to remove detached cells, fresh medium containing 2% FBS with or without EVs was added. Wound closure was monitored and imaged at 0, 12, and 24 h. The migration rate was calculated as:

$$Migration\ rate\ (\%) = (A_0 - A_t) / A_0 \times 100\% \quad (1)$$

where A_0, and A_t represent the initial wound area and the remaining area at time t, respectively. All experiments were performed with at least three biological replicates.

Neutral Lipid Content Assay

Neutral lipid droplets were stained with BODIPY 493/503. Cells were incubated with 1 μg mL^{-1} BODIPY for 30 min, washed, and counterstained with DAPI. Fluorescence images were acquired and analyzed for mean intensity using ImageJ.

Injectability and self-healing properties of DCH hydrogels

The rheological properties of the hydrogels were characterized using a rheometer. The storage modulus (G′) and loss modulus (G″) of the hydrogel were measured under an oscillatory frequency sweep from 0.6 to 100 rad s^{-1} at a constant strain of 1%. To determine the linear viscoelastic region of the hydrogels, strain amplitude sweeps were performed from 0.1% to 1000% at a fixed frequency of 1 Hz. To further investigate the self-repairing properties of the hydrogel, oscillatory strain was applied at 1 Hz, alternating from small strains (γ = 1.0%) to large strains (γ = 1000%), for 5 cycles. The viscosity and shear-thinning behavior were characterized by rotational shear rate sweeps from 0.1 to 100 s.

To further visually demonstrate injectability, the hydrogel was loaded into a syringe and continuously extruded in different patterns, with photographic recording. To assess its self-healing properties, the hydrogel was cut into two flaps with tweezers, stained with methylene blue and rhodamine B, respectively, and then the flaps were placed in contact with each other to monitor interfacial recovery before and after self-repair.

Cytocompatibility of DCH@EVs hydrogels

The cytocompatibility of the hydrogels was evaluated by live/dead staining. First, NIH3T3 cells were digested and collected by centrifugation. Then, the cells were seeded in 24-well plates (4×104 cells per well) and incubated for 24 h at 37 ° C, 5% CO2. After adhesion, the medium was replaced, and cells were co-incubated with Control, DCH-gel, UCMSCs-EVs, or DCH@EVs hydrogel for 24 h. Subsequently, the cells were washed three times with PBS and stained with calcein-AM (green fluorescence) and propidium iodide (PI, red fluorescence) in the dark conditions for 15 min. Fluorescence images of live and dead cells were obtained by fluorescence microscopy (ZEISS), and the number of live cells in each group was quantitatively analyzed.

Antioxidant properties of DCH@EVs hydrogels *in vitro*

The ROS-scavenging properties of different hydrogels were evaluated in BMDMs under oxidative stress using the 2',7'-dichlorodihydrofluorescein diacetate (DCFH-DA) probe and dihydroethidium (DHE) probe. Firstly, the digested and collected BMDM were seeded in 24-well plates at a density of 4×10^4 cells per well and incubated for 12 h. Then, 10 μg mL^{-1} ROSup was added to the medium to induce oxidative stress for 30 min. Then, cells were co-incubated with Control, DCH-gel, UCMSCs-EVs, or DCH@EVs hydrogel for 12 h. After incubation, the cells were rinsed thrice with sterile saline. Then, the cells were stained with 10 μM DCFH-DA or DHE in the dark for 30 min. Finally, fluorescence images were captured using a fluorescence microscope to assess intracellular ROS content and superoxide ($^{\bullet}O_2^-$) levels.

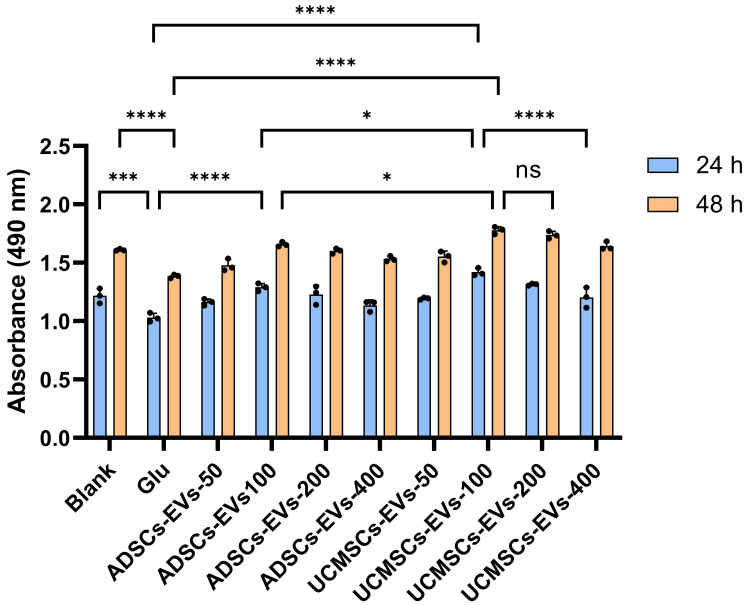

1

2 **Figure S1**. MTT assay results. Cell viability in different dose of EVs (μg mL^{-1})

3 treatment in NIH-3T3 was assessed by MTT assay.

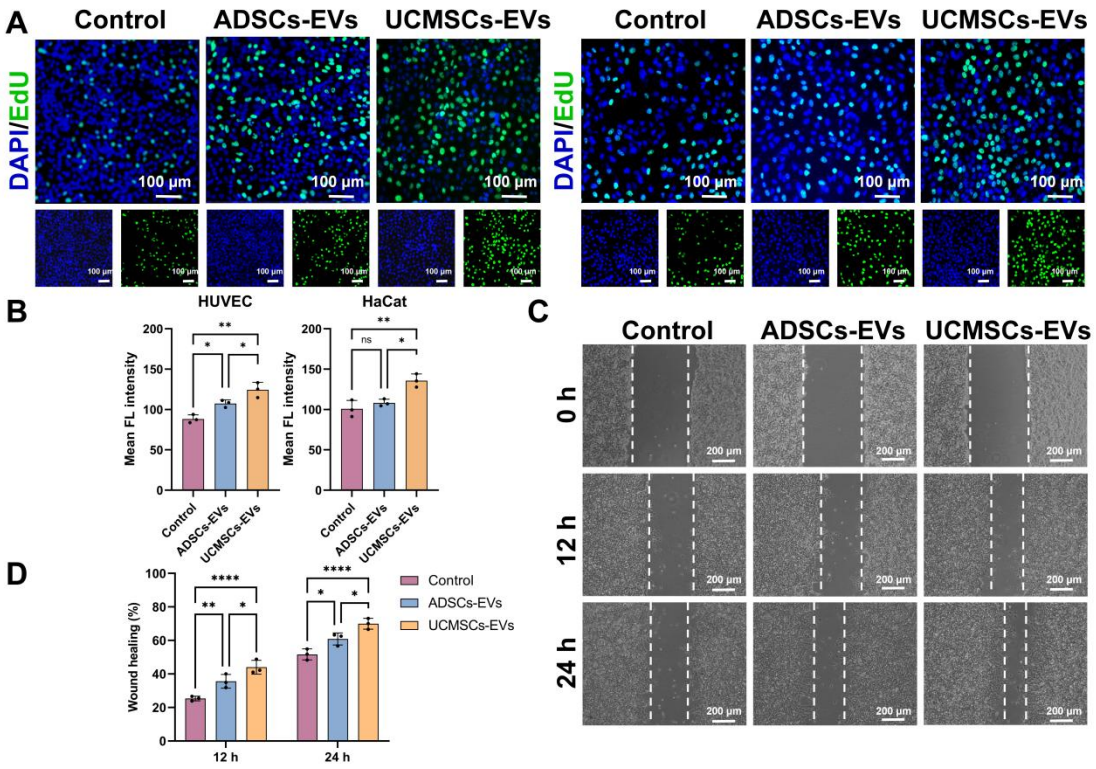

Figure S2. UCMSC-EVs exhibit stronger pro-reparative activity than ADSC-EVs *in vitro*. EdU staining was performed to evaluate the effects of ADSC-EVs and UCMSC-EVs on the proliferation of HUVECs (left) and HaCaT cells (right) under high-glucose conditions. Green fluorescence indicates EdU-positive proliferating cells, and blue fluorescence indicates DAPI-stained nuclei. (B) Quantitative analysis of EdU-positive fluorescence intensity, n = 3. (C) A scratch wound assay was conducted to assess the effects of ADSC-EVs and UCMSC-EVs on NIH3T3 cell migration. (D) Quantitative analysis of the migration rate of NIH3T3 cells at 12 h and 24 h, n = 3.

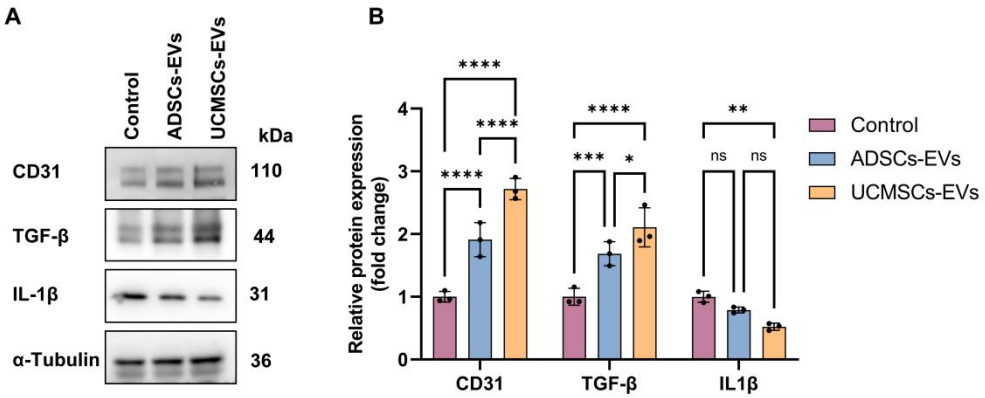

Figure S3. UCMSC-EVs markedly accelerate wound healing in a diabetic mouse model. Western blot analysis of CD31, TGF-β, and IL-1β protein expression in diabetic wounds treated with ADSC-EVs or UCMSC-EVs. (B) Quantitative analysis of CD31, TGF-β, and IL-1β protein levels, n = 3.

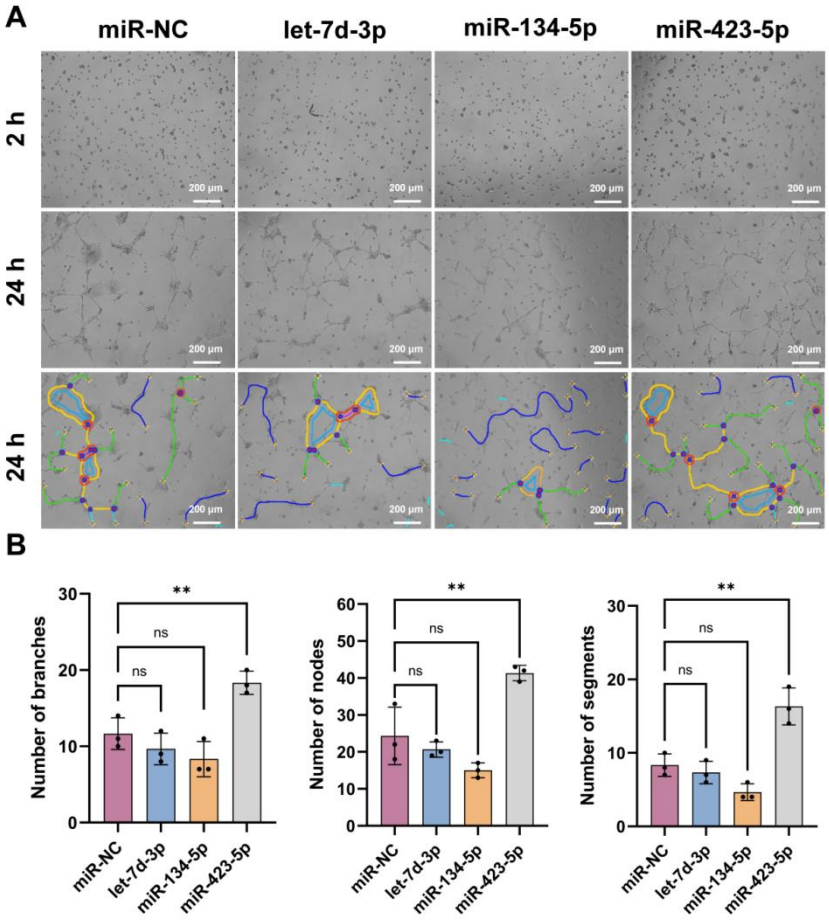

Figure S4. Effects of let-7d-3p, miR-134-5p, and miR-423-5p on *in vitro* angiogenesis. (A) Matrigel tube formation assays were performed to assess the effects of let-7d-3p, miR-134-5p, and miR-423-5p transfection on the angiogenic capacity of HUVECs *in vitro*. (B) Quantitative analysis of the numbers of branches, nodes, and segments formed by HUVECs, n = 3.

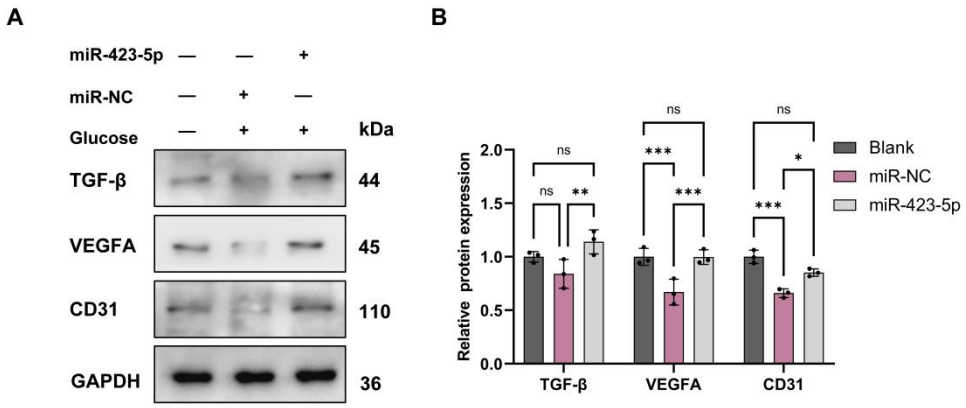

Figure S5. Effects of miR-423-5p on angiogenesis-related factors under high-glucose conditions. (A) Western blot analysis of CD31, TGF-β, and VEGFA protein expression in HUVECs transfected with miR-423-5p under high-glucose conditions. (B) Quantitative analysis of CD31, TGF-β, and VEGFA protein levels, n = 3.

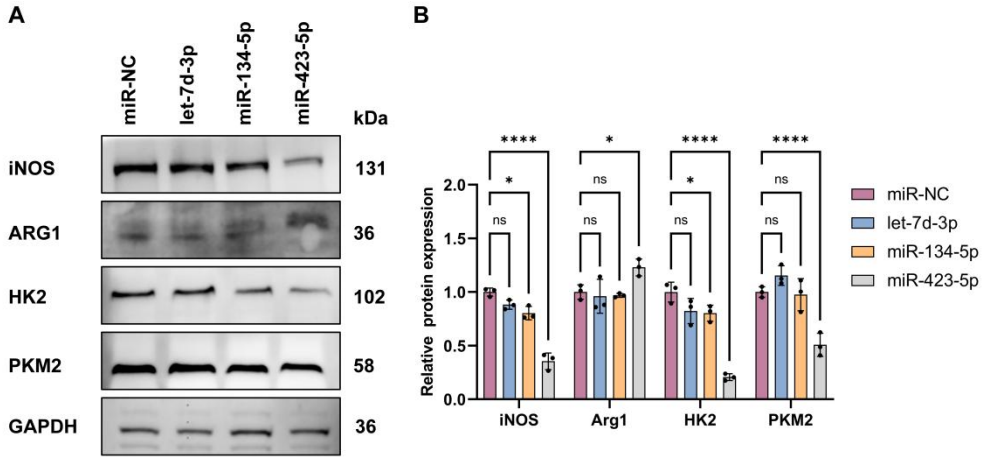

Figure S6. Effects of let-7d-3p, miR-134-5p, and miR-423-5p on glycolysis and polarization in BMDMs. (A) Western blot analysis of iNOS, Arg1, HK2, and PKM2 protein expression in BMDMs co-incubated with LPS and let-7d-3p, miR-134-5p, or miR-423-5p. (B) Quantitative analysis of iNOS, Arg1, HK2, and PKM2 protein levels, n = 3.

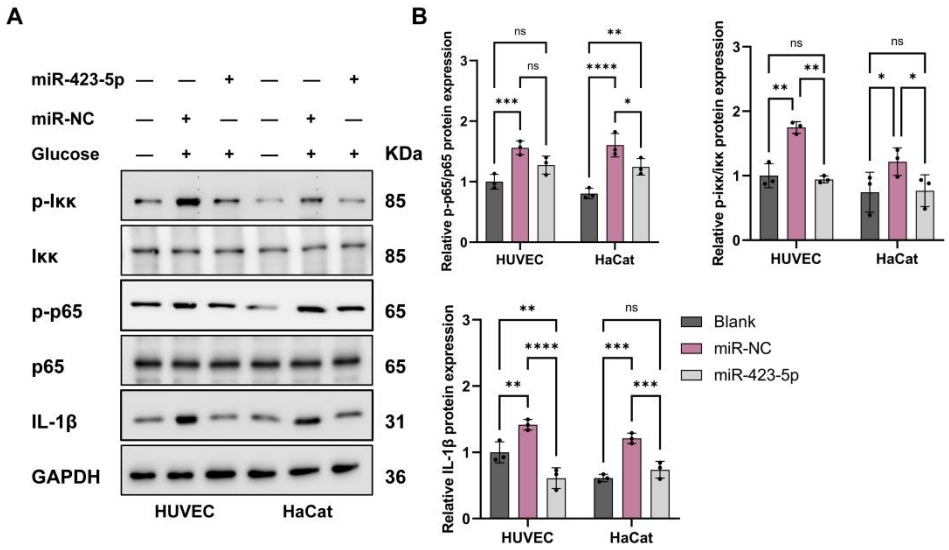

Figure S7. Effects of miR-423-5p on the NF-κB signaling pathway under high-glucose conditions. (A) Western blot analysis of p-p65, p-Iκκ, and IL-1β expression in HUVECs and HaCaT cells cultured under high-glucose conditions. (B) Quantitative analysis of p-p65, p-Iκκ, and IL-1β protein levels, n = 3.

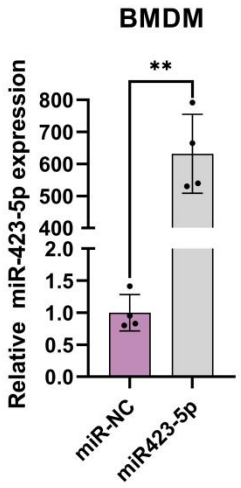

Figure S8. RT-qPCR analysis was performed to determine the transfection efficiency of the miR-423-5p mimic in BMDMs, n = 3.

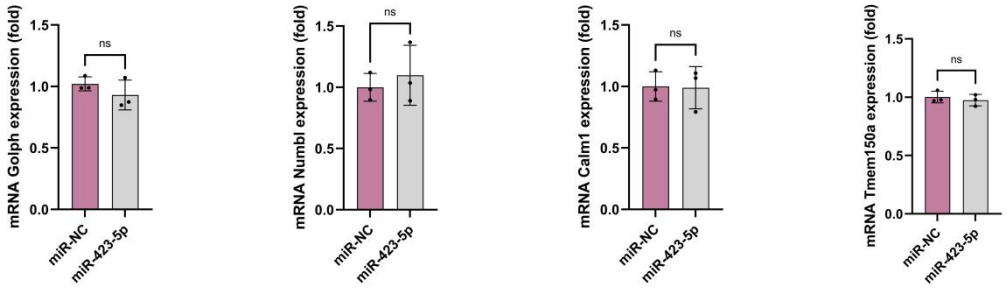

Figure S9. Prediction of target genes of miR-423-5p in BMDMs. RT-qPCR analysis of the expression of Golph, Numbl, Calm1, and Tmem150a in BMDMs following transfection with the miR-423-5p mimic, n = 3.

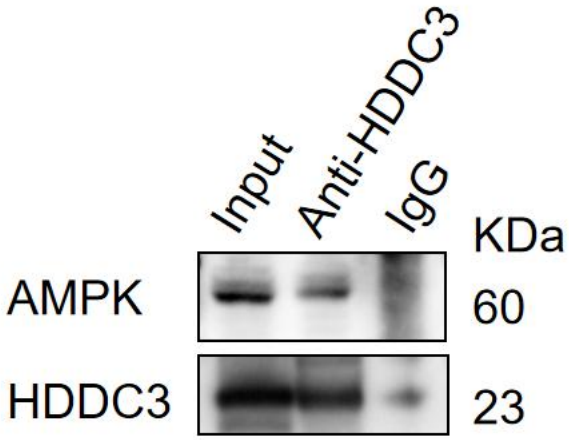

Figure S10. HDDC3 associates with AMPK as determined by co-immunoprecipitation. HEK293T cells overexpressing HDDC3 were subjected to co-immunoprecipitation using an anti-HDDC3 antibody or control IgG, followed by immunoblotting for AMPK and HDDC3.

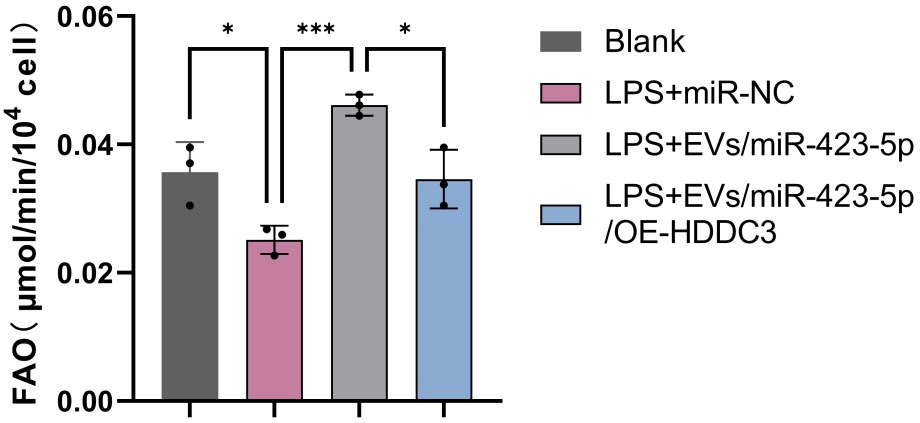

Figure S11. Measurement of FAO rate in BMDMs. Changes in the FAO rate in BMDMs under different treatment conditions. n=3.

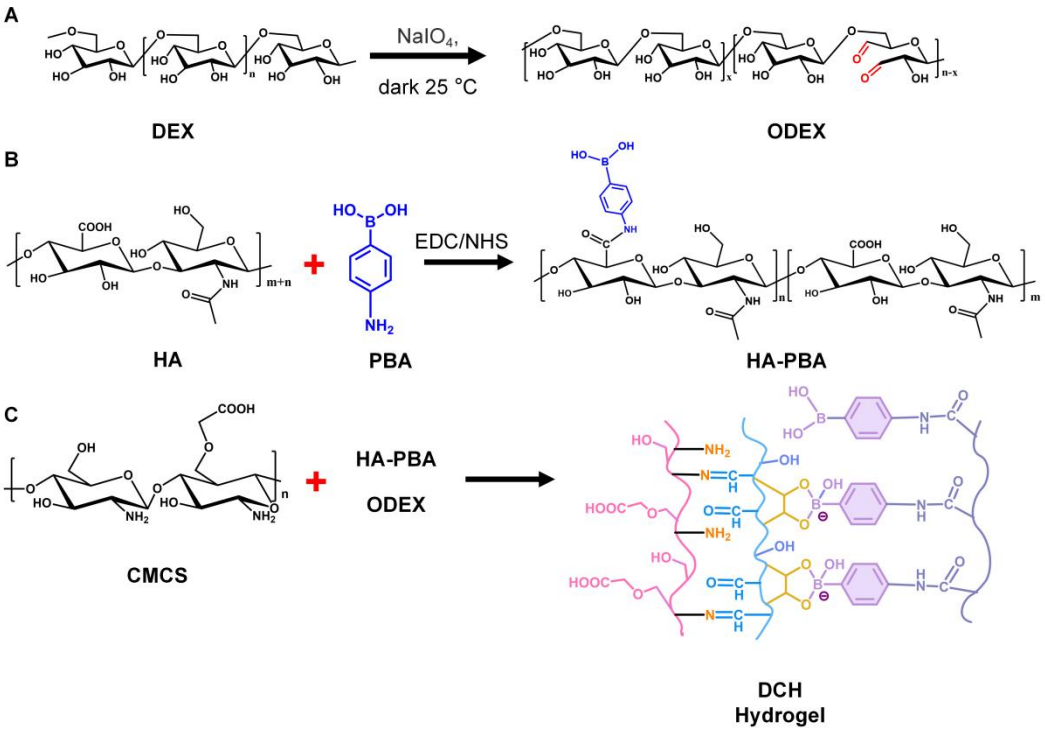

Figure S12. Synthetic routes of the DCH hydrogel. Synthesis of (A) oxidized dextran, (B) HA-PBA, and (C) the DCH hydrogel.

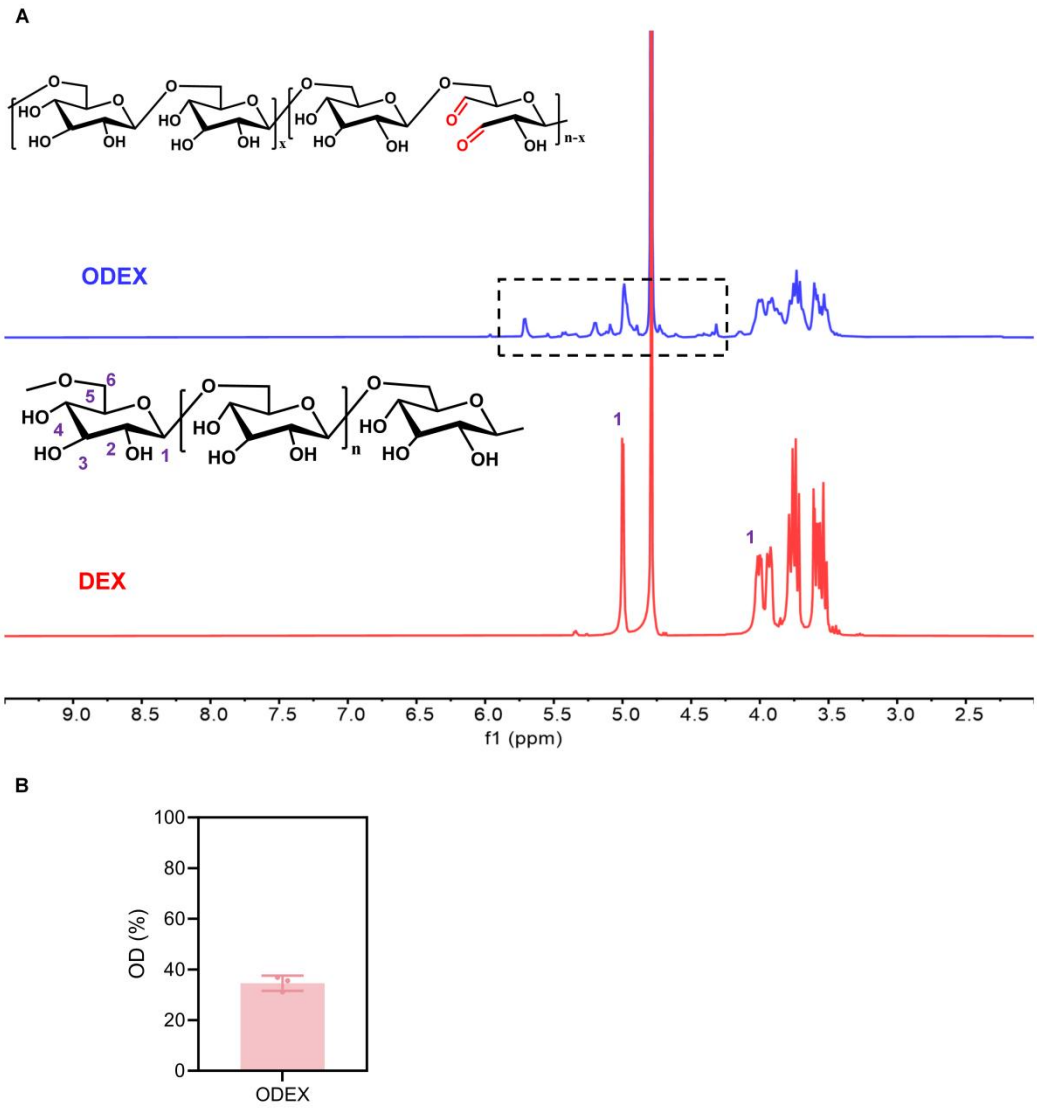

Figure S13. (A) The ^{1}H NMR spectrum of oxidized-dextran (400 MHz, D_2O). (B) Degree of oxidation of oxidized-dextran.

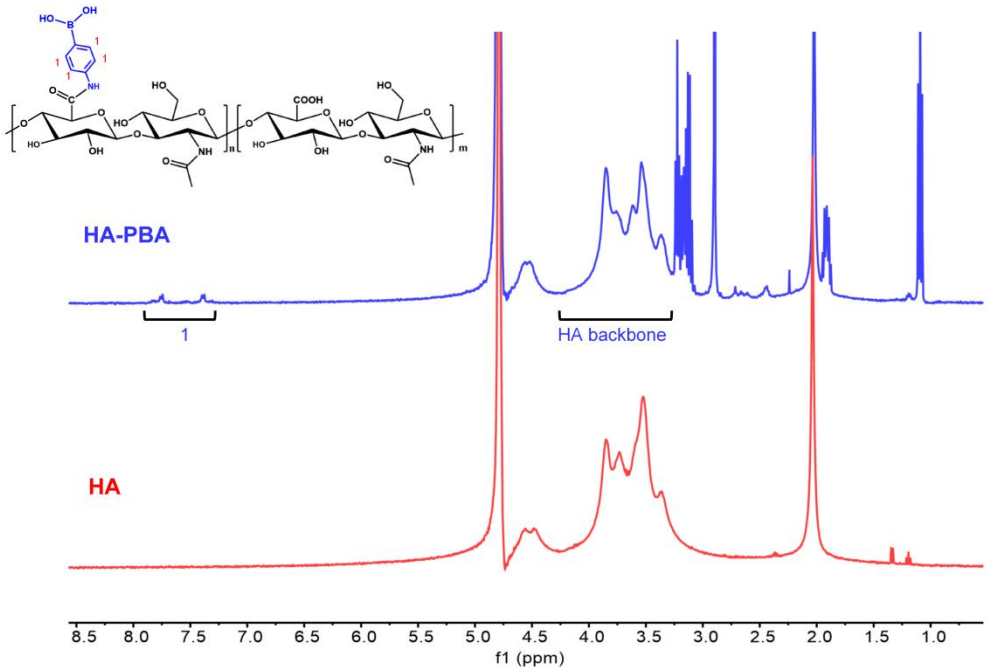

Figure S14. The ^{1}H NMR spectrum of HA-PBA (400 MHz, D_2O).

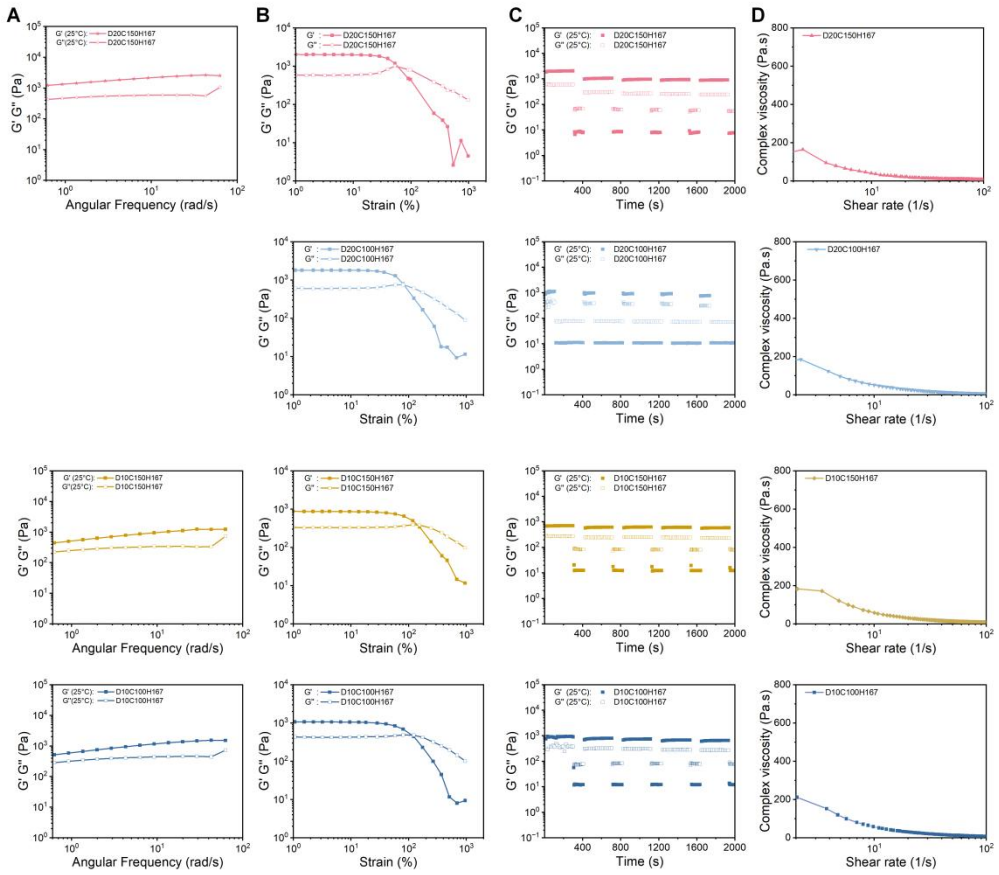

Figure S15. (A) The frequency-scan curve of the different hydrogels. (B) The shear-strain scanning curves of the different hydrogel. (C) Self-healing property of the different hydrogel under dynamic strain cycling test. (D) Shear-thinning behavior of the different hydrogel.

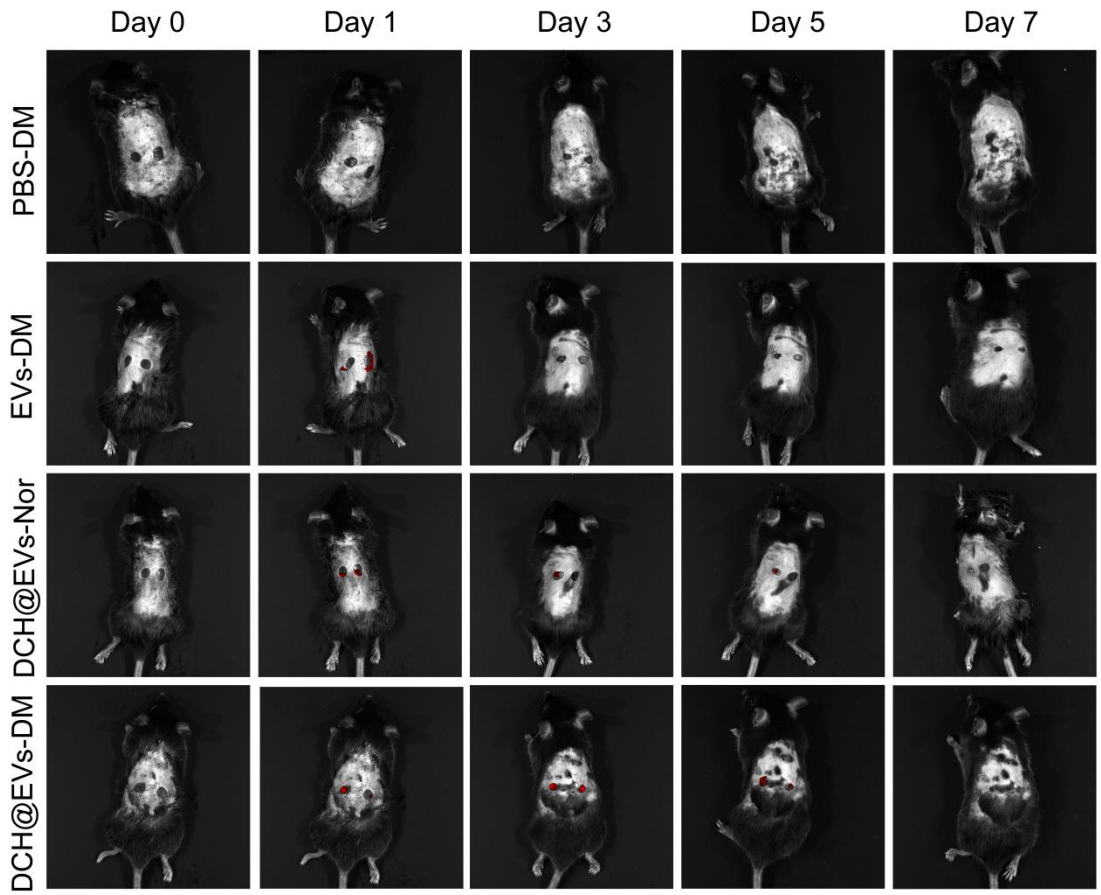

Figure S16. *In vivo* fluorescence tracking of free and DCH hydrogel-encapsulated PKH26-labeled EVs in normal and diabetic mouse wounds.

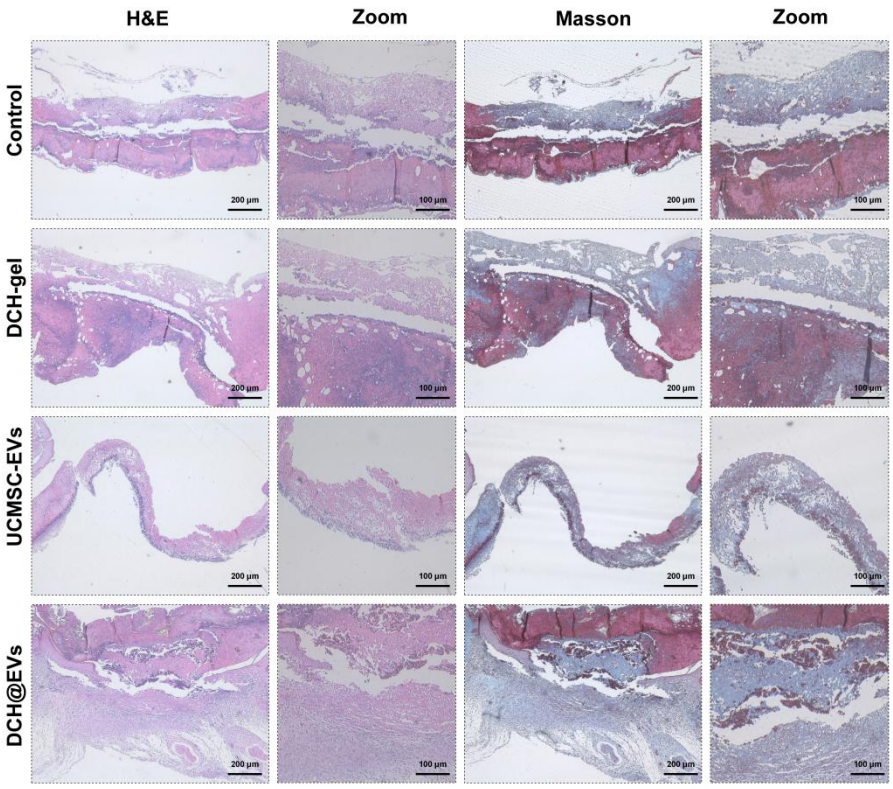

Figure S17. Histological evaluation of wound skin tissues in diabetic mice on day 7.

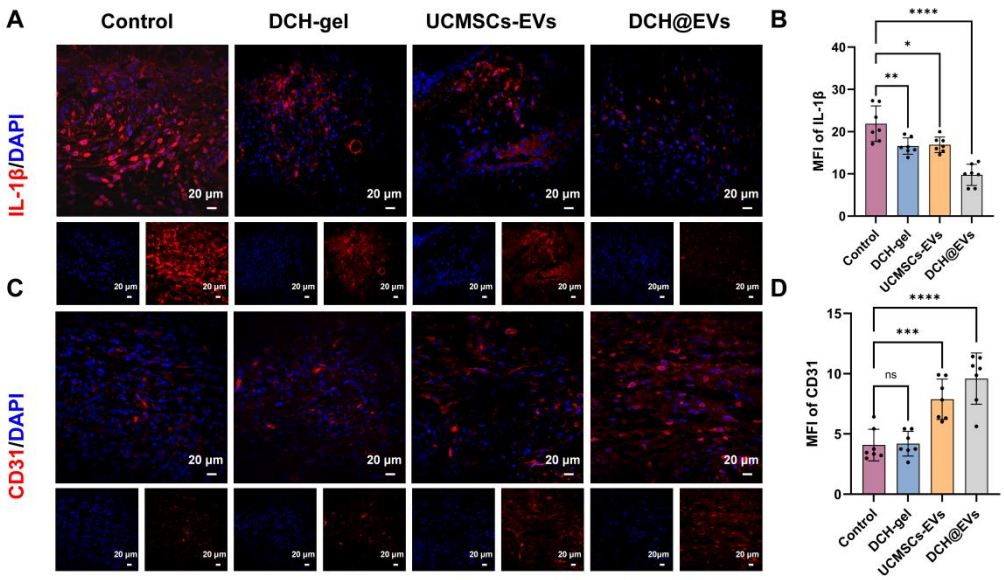

Figure S18. A DCH@UCMSCs-EVs hydrogel synergistically promotes diabetic wound healing *in vivo*. Immunofluorescence staining of IL-1β in wound skin tissues from diabetic mice on day 7. Red fluorescence indicates IL-1β protein, and blue fluorescence indicates DAPI-stained nuclei. (B) Immunofluorescence staining of CD31 in wound skin tissues from diabetic mice on day 7. Red fluorescence indicates CD31 protein, and blue fluorescence indicates DAPI-stained nuclei. (C) Quantification of the fluorescence intensity for IL-1β and CD31 (D), n = 7.

Table S1. List of primer sequences

Gene	Forward primer (5'-3')	Reverse primer (5'-3')
Arg1	CAGCACTGAGGAAAGCTGGT	ACAGACCGTGGGTTCTTCAC
iNOS	TACTGAGACAGGGAAGTCTGAA	AGTAGTTGCTCCTCTTCCAAGGT
Hddc3	CCGCTCACAAACACCGACA	GCGGCCTGTAACACCACAA
Golph	ACAAGGGCGACTCCAAGGA	ATGATGTGTAACCCTCTCGGT
Numbl	GCAGGCACCATGAACAAGTTA	TCTTCACAAACGTGCATTCCC
Calm1	TGGGAATGGTTACATCAGTGC	CGCCATCAATATCTGCTTCTCT
Tmem150a	TGGTCCTACAATGAATCCTGCT	TGAGTGCAGTGGTATTGATCCA
Gapdh	TGGATTTGGACGCATTGGTC	TTTGCACTGGTACGTGTTGAT
miR-423-5p	GenePharma China	UGAGGGGCAGAGAGCGAGACUUU
let-7d-3p	GenePharma China	CUAUACGACCUGCUGCCUUUCU
miR-134-5p	GenePharma China	UGUGACUGGUUGACCAGAGGGG

Table S2. Antibodies information

Antibodies	Brand	Catalog Number	Dilution ratio
CD105	Abcam	ab156756	1:1000
CD73	Abcam	ab317462	1:1000
CD90	Abcam	ab307736	1:500
CD34	Abcam	ab81289	1:5000
CD45	Abcam	ab40763	1:500
HLA-DR	Abcam	ab91334	1:1000
CD63	Abcam	ab254011	1:2000
TSG101	Thermo	MA5-48613	1:2000
CD81	Thermo	MA5-32333	1:500
CD31	Proteintech	28083-1-AP	1:2000
TGF-β	Proteintech	81746-2-RR	1:2000
FGF2	Proteintech	11234-1-AP	1:1000
GAPDH	Proteintech	60004-1-Ig	1:50000
ARG1	ABclonal	A1847	1:1000
INOS	Abcam	ab178945	1:5000
α-Tubulin	Proteintech	11224-1-AP	1:10000
IL-1β	Proteintech	16806-1-AP	1:2000
VEGFA	Proteintech	66828-1-Ig	1:2000
HK2	Abcam	ab104836	1:1000
PKM2	ABclonal	A20991	1:100-

p-Iκκ	ABclonal	AP0891	1:1000
Iκκ	Proteintech	15649-1-AP	1:1000
p-p65	ABclonal	AP0124	1:1000
p65	Proteintech	66535-1-Ig	1:2000
PGC-1α	ABclonal	A20995	1:2000
CPT1α	ABclonal	A27657	1:1000
p-AMPK	Proteintech	80209-6-RR	1:1000
AMPK	Proteintech	10929-2-AP	1:2000
p-MTOR	Proteintech	80596-1-RR	1:1000
MTOR	Proteintech	20657-1-AP	1:2000
HDDC3	Proteintech	21091-1-AP	1:2000

1